Journal of Enhanced Heat Transfer, 27(2):173–194 (2020)

EXPERIMENTAL AND NUMERICAL STUDY OF TWO-PHASE FLOW IN A RECTANGULAR MINI-CHANNEL WITH SUDDEN EXPANSION STRUCTURE

Shuangting Liu,[1] Yonggang Jiao,[2,] Bo Gao,[3] & Bin Liu[4]*

Shijiazhuang Tiedao University, College of Mechanical Engineering, Shijiazhuang 050043, China

*Address all correspondence to: Yonggang Jiao, Shijiazhuang Tiedao University, College of Mechanical Engineering, Shijiazhuang 050043, China, E-mail: jyg76@sohu.com

Original Manuscript Submitted: 11/23/2019; Final Draft Received: 1/6/2020

The mini-channel heat sink is widely seen as a promising heat exchanger owing to its high efficiency and small size. In order to design an optimal structure and enable its operation at high efficiency, it is critical to predict the two-phase pressure drop for this type of channel. In this study, the pressure drop through a single rectangular mini-channel with sudden expansion is measured, and five primary flow patterns, bubble flow, slug flow, plug flow, jetlike flow, and annular flow, are observed by visualization experiments. A computational fluid dynamics model is also proposed for them. It is found that the pressure gradient on the bubble surface is very large, and the pressure drop of gas-liquid flow is closely related to the flow pattern. A new frictional pressure drop prediction model is also proposed using a modified parameter C with the effects of small channel diameter, viscosity, surface tension, mass velocity, flow pattern, and flow regime. Also, the new correlation has a better performance in predicting the two-phase frictional pressure drop within a wide range of mass flux.

KEY WORDS: *mini-channel, pressure drop, two-phase, heat transfer enhancement, simulation, visualization*

1. INTRODUCTION

The rectangular mini-channel heat sink has attracted increasing attention owing to its fairly compact structure and its high efficiency in heat transfer. Therefore, it is well adapted for cooling precision instruments with high heat flux such as electronic chips. Many scholars have made in-depth studies on mini-channel heat sinks from the aspects of working medium, heat transfer form, structure, and so on. Alejandro et al. (2015) found that nonuniform flow in a multiport mini-channel tube yielded a lower overall heat transfer coefficient. Guan et al. (2019) studied the influence of contact angle on enhanced heat transfer, and Nandakrishnan et al. (2018) focused their attention on the application of improved heat transfer properties of Al_2O_3-water nanofluids when used in conjunction with a diverging micro-channel with a staggered dimpled surface to improve overall heat transfer characteristics. Tiwari and Manoj (2019) made an improved design of a raccoon micro-channel heat sink which had an additive effect on the thermal performance, and Guo (2019) reviewed papers on heat transfer enhancement published in 2018 and

1065–5131/20/$35.00

NOMENCLATURE

Bo	Bond number given in Eq. (13)	ΔP_{exp}	pressure drop in the present experiments
C	Chisholm parameter	ΔP^*_{exp}	pressure drop in the published literature's experiments
Ca	capillary number given in Eq. (26)	Re	Reynolds number
$C_1, C_2,$ C_3, C_4	constant	T	temperature (°C)
D_h	hydraulic diameter (m)	We	Weber number given in Eq. (12)
e	relative error (%)	X	Lockhart-Martinelli parameter
Fr	Frond number	x	gas quality ratio
G	mass velocity (kg/m^2·s)		
g	gravitational acceleration		
j	superficial velocity (m/s) or the average velocity of two-phase flow	**Greek Symbols**	
K	loss coefficient	Ω_{c1},Ω_{c2},Ω_{c3}	correction factors of sudden contraction
l_c	Laplace constant	Ω_{e1},Ω_{e2},Ω_{e3}	correction factors of sudden expansion
MAE	mean absolute error (%)	β	volume fraction of gas
N^{conf}	confinement number	ρ	density (kg/m^3)
ΔP	pressure drop (Pa, kPa)	μ	viscosity (Ns/m^2)
ΔP_{c1}	pressure drop of the sudden contraction given in Eq. (10)	ν	specific volume (m^3/kg)
		σ	surface tension (N/m)
ΔP_{cHom}	pressure drop model of the sudden contraction based on the homogeneous model, given in Eq. (11)	**Subscripts**	
		c	contraction
		$c1$	contraction structure inlet
		$c2$	contraction structure outlet
$\Delta P_{e1}, \Delta P_{e2},$ ΔP_{e3}	pressure drop of the sudden expansion given in Eq. (14)	e	expansion
		G	gas-phase
ΔP_{eHom}	pressure drop model of the sudden expansion bases on the homogeneous model, given in Eq. (15)	in	test module inlet
		L	liquid-phase
		Lo	liquid only
		out	test module out
$\Delta P_{F1}, \Delta P_{F2},$ ΔP_{F3}	pressure drop of two-phase flow in the straight channel	pred	predicted
		$p1, p2$	deep, shallow plenum
ΔP_{pred}	predicted pressure drop, given in Eq. (9)	TP	two-phase
		VV	laminar liquid-laminar gas

found that phase-change heat transfer was one of the hot spots in the study of enhanced heat transfer. Although the relevant research on enhanced heat transfer about a mini-channel is relatively comprehensive, there are two problems that still hinder the development of the application of the mini-channel. One is the high pressure drop of the mini-channel heat sink owing to its

extremely small hydraulic diameter, high viscosity, and surface tension. The other is the flow of the two-phase mixture across singularities such as sudden expansions and contractions, which is commonly seen in connection channels and is relevant to many applications such as mini power generation units and mini chemical reactors. Therefore, the accurate prediction of pressure drop in two-phase flow through a mini-channel with sudden expansion and contraction structure is critical for designing heat sinks.

To predict the pressure drop in a sudden expansion, Chen et al. (2007) and Ahmed et al. (2006) studied the flow patterns and pressure drop of two-phase flow through sudden expansion, and analyzed existing prediction formulas for sudden expansion in macro-channels. They found that most pressure drop prediction formulas used in macro-channels were inaccurate. Wang et al. (2010) collected available data from five publications and proposed a more accurate formula to predict pressure drop across a sudden expansion in a mini-channel. Their formula was compared with the calculations recommended by Wadle's correlation (1989), Schmidt and Friedel's correlation (1994), and Attou and Bolle's correlation (1997). They found that the accuracy of pressure drop predictions for sudden expansion based on a homogeneous model was poor, and the prediction formula was modified and then the average error reached 23%.

As for a sudden contraction, Chen et al. (2008a) have examined the flow characteristics of two-phase (air-water) flow across contractions which were from a small rectangular channel (3×6 mm and 3×9 mm) into a round tube with a diameter of 3 mm. Their experimental data of pressure drop across the contractions were compared with the calculations by a homogeneous flow model recommended by Schmidt and Friedel's correlation (1997) and Abdelall et al.'s correlation (2004). The results from the homogeneous flow model were in good agreement with their data. On the basis of the above research, Chen et al. (2008b) also investigated contractions of different size which were from small rectangular channels (2×4 mm, 2×6 mm, 4×4 mm, and 4×6 mm) into a round tube with a diameter of 2 mm, respectively. Based on their data, a modified homogeneous model was proposed to predict the pressure drop across contractions and the mean deviation reached 30%.

However, Lee et al. (2017) studied the pressure drop characteristics of large length-to-diameter two-phase mini-channel heat sinks under the condition of boiling. They found that two-phase frictional pressure drop is the most dominant of five components: two-phase frictional pressure drop, pressure drop associated with two-phase acceleration, pressure drop at inlet contraction, pressure drop from upstream single-phase liquid flow, and pressure drop from outlet recovery. Also, many parameters could affect frictional pressure drop significantly, such as mass velocity and flow patterns. Choi et al. (2010) found that the aspect ratio of a rectangular channel directly affected the flow patterns, and indirectly affected the pressure drop. They concluded that the frictional pressure drop in the rectangular mini-channel was highly related to the flow patterns. Lei and Chen (2019) drew a similar conclusion by studying the annular transition flow regime by experimental and numerical methods. They also found that annular flow was a complex and extremely unstable flow. Lee et al. (2017), Qu and Siu-Ho (2009), Kim and Mudawar (2012), and Xiao et al. (2018) evaluated the frictional pressure drop in mini-channels using a separated flow model and a homogeneous equilibrium flow model. They applied their new approaches to predict a two-phase frictional pressure drop by modifying the parameter C which originated from Lockhart and Martinelli's correlation (1949). Their predicted results showed good agreement with experimental results when the optimal value of C was utilized, which proved that modifying parameter C can improve the accuracy of pressure drop prediction. Then their method became the mainstream for predicting parameter C. Mishima and Hibiki (Mishima et al., 1993) investigated the relationship between the value of C and hydraulic diameter, and

proved that the value of C was related to channel size. English and Kandlikar (2006) studied the surfactant effect on air-water flow in mini-channels. They stated that Mishima and Hibiki's correlation (Mishima et al., 1993) did not fit the laminar-laminar (VV) flow condition. Therefore, they proposed a modified correlation which supported a lower value of C in the VV condition. The laminar (liquid)–laminar (gas) flow condition is a common phenomenon in two-phase flow in mini-channels, which was identified by Zhang et al. (2009). They also studied the distribution of all adiabatic data points from other existing literature in the plot of Re_f versus Re_g, and found few data on the turbulent-turbulent (TT) condition. It also can be inferred from the definition of the Reynolds number. A low Reynolds number results from the reduction on flow rate due to the high pressure drop and the inherently small dimensions of mini-channels. Therefore, they concluded that the flow in a mini-channel has the characteristics of laminar flow. Zhang et al. (2009), Li and Hibiki (2017), and Sempértegui-Tapia and Ribatski (2017) collected data from existing databases and formulated their own correlations for parameter C which are functions of the two-phase Reynolds number Re_{tp}, two-phase viscosity number $\mathrm{N}_{\mu tp}$, vapor quality x, and the effect of the geometry, but no flow patterns. Fu et al. (2010) studied the flow pattern formation mechanism of gas-liquid flow in mini-channels. They found that the viscous force and surface tension were the dominant factors controlling flow pattern formation. The Ca value representing the relative importance of viscous force and surface tension is proposed to predict the flow pattern formation mechanism. To further improve the accuracy of frictional pressure drop prediction, this paper proposes a new correlation that takes into account the effects of Reynolds number, geometry, mass velocity, and the flow patterns through introducing the capillary number (Ca).

At present, many scholars use numerical simulation methods to study mini-channels, but most are concerned with the steady-state model for single-phase fluids or nanofluids. For example, Chai et al. (2016) and Sahar et al. (2017) studied the effect of mini-channel structure on flow and heat transfer characteristics by simulating steady-state single-phase flow. Kumar and Sarkar (2018, 2019) studied the hybrid nanofluid characteristics in small channels by experiments and numerical simulations. Gas-liquid flow in a mini-channel is an extremely unstable process, and few scholars have used transient numerical and experimental methods to analyze it. Although Wu et al. (2018) and Wei (2017) studied gas-liquid flow by experimental or numerical methods, few scholars have studied two-phase flow by combining experiments and simulations. One exception is Abood et al. (2019), who noted a convergence between experimental and numerical results in the flow patterns. It means that it is feasible to study two-phase flow in mini-channels by experiments and simulations.

This study is to develop a suitable numerical model using FLUENT for two-phase flow in a horizontal rectangular mini-channel with sudden expansion. By simulations and experiments, the relationship between pressure drop and flow patterns is considered comprehensively, and a more comprehensive frictional pressure drop prediction formula is proposed. Furthermore, this paper compares the accuracy and applicability of the new correlation with the existing correlations and databases.

2. EXPERIMENTAL METHOD

2.1 Experimental Setup

Figure 1 shows a schematic diagram of the two-phase cooling loop which was configured to conduct the working fluid, i.e., the mixture of nitrogen gas and liquid water, to the desired operating

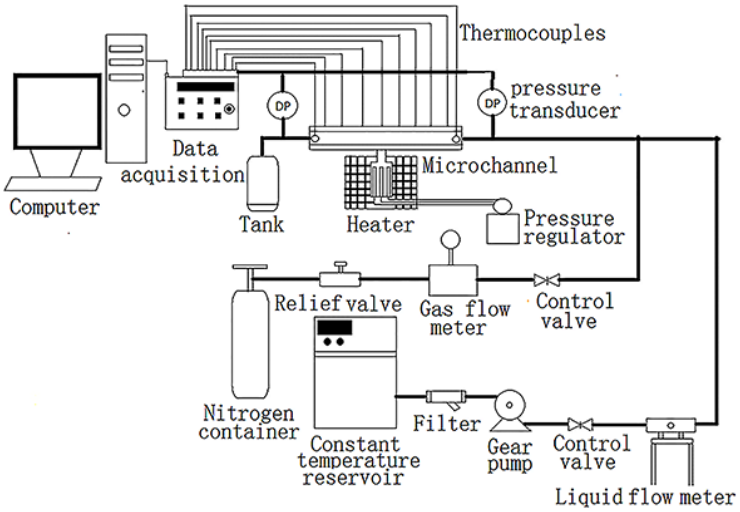

FIG. 1: Schematic diagram of two-phase loop: (a) front view, (b) side view, (c) dimensional drawing

conditions. Nitrogen was supplied from the nitrogen container passing through a control valve. It was adjusted depending on the flow pattern change in the mini-channel, and the flow rate was measured by a gas flow meter. The water flow loop consists of a gear pump that delivers water to a constant temperature reservoir to maintain the test module's temperature at 26°C, and a liquid flow meter which measures the flow quality of the water when an important flow pattern or flow state appears in the mini-channel.

As shown in Fig. 2, the mini-channel was cut into the 85-mm-long and 25-mm-wide top surface of an oxygen-free copper block. The test module consists of a cover plate and a mini-slot which has an expansion structure expanding suddenly from 1×1 mm to 1×4 mm. Within this module, the top of the test module was closed off by a transparent cover plate so that the flow patterns in the mini-channel could be visualized.

The inlet and outlet of the mini-channel module were measured by pressure transducers. In order to accurately measure the pressure drop at the inlet and outlet, three kinds of pressure transducers with ranges of 0–6, 0–10, and 0–20 kPa were used in this experiment. Both the pressure measurements and high-speed video analysis were performed with the mini-channel module. The data acquisition in the experimental system was used to collect signals from the pressure transducers and flow meters. The experimental conditions and ranges are summarized in Table 1. The Reynolds number for liquid or gas is determined by their superficial velocity, respectively.

2.2 Uncertainty Analysis

To assess the reliability of the experimental data, an uncertainty analysis was carried out using the theory of the propagation of error (Moffatt, 1988). The uncertainty U_F on a quantity F which is function of $x_1, \ldots, x_n$. And the measured variables' uncertainty U_{xi} can be calculated as formula (1). It was also used for experimental research by Heyhat et al. (2013) and Zhai et al. (2017).

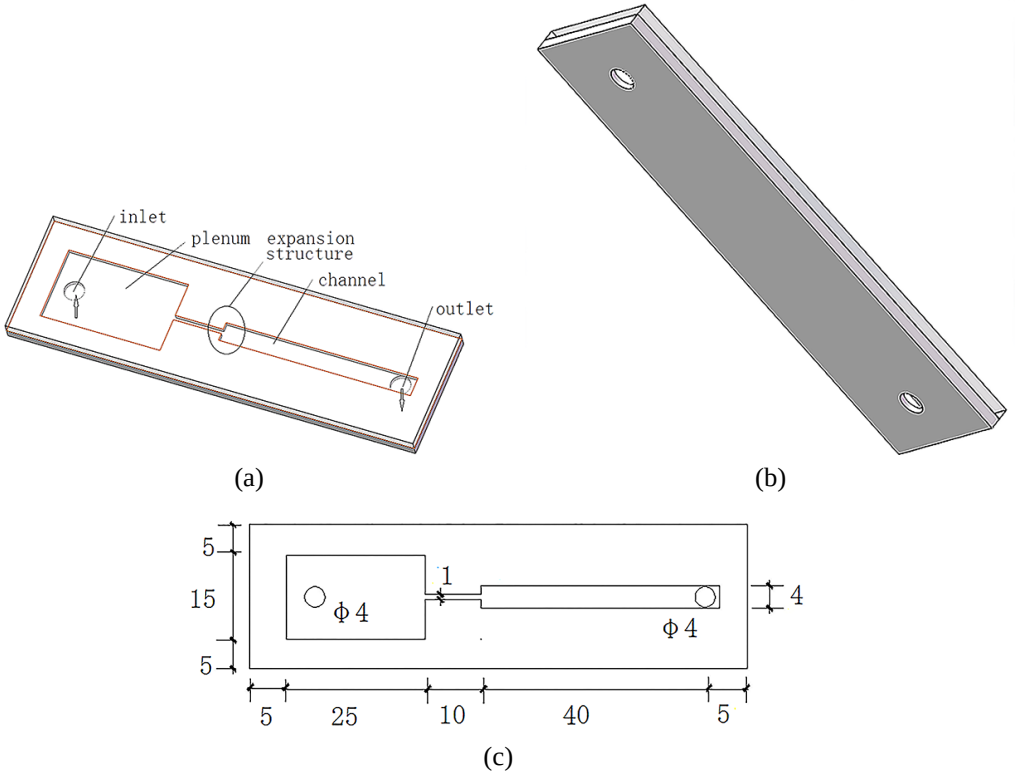

FIG. 2: Test module

TABLE 1: The experimental conditions and ranges

Variables	Ranges
Hydraulic diameter, D_h ($W_{ch} \times H_{ch}$) (mm)	1 × 1 expand to 1 × 4
Pressure drop (kPa)	0.658–11.401
Liquid mass flux, G_L (kg/m^2·s)	332.73–1330.93
Gas mass flux, G_G (kg/m^2·s)	0.1103–2.253
Liquid superficial velocity, j_L (m/s)	0.026–0.106
Gas superficial velocity, j_G (m/s)	0.007–0.146

$$U_F = \pm \sqrt{\sum_{i=1}^{n} \left(\frac{\partial F}{\partial x_i} U_{xi} \right)^2}. \tag{1}$$

The relative uncertainties of basic parameters are shown in Table 2.

TABLE 2: Relative uncertainty of parameters

Parameters	Values
Relative uncertainty of the gas flow rate	3.21%
Relative uncertainty of the liquid flow rate	3.33%
Relative uncertainty of the pressure drop	2.52%

3. NUMERICAL SIMULATIONS

3.1 Conservation Equations and Numerical Method

A three-dimensional nitrogen-water conjugate model was used to predict flow performance for the mini-channel using FLUENT in this paper. The volume of fluid (VOF) model was used to track and locate the shape and position of the interface between two or more immiscible fluids. The laminar model was considered because even in the annular flow regime, the liquid-only Reynolds number (Re_{Lo}) and the gas-only Reynolds number (Re_{Go}) are small owing to the small channel size. In order to simplify the module simulation, the following assumptions are made:

(1) three-dimensional, transient state, laminar, no slipping flow;

(2) adiabatic flow;

(3) constant physical properties for fluids and solids;

(4) incompressible Newtonian fluid gas and liquid are mixed evenly at the inlet;

(5) reasonable flow continuum and Navier–Stokes (N-S) equation.

The continuity, momentum, and gas volume fraction (β) conservation equations can be written as

$$\frac{\partial \overrightarrow{V}}{\partial t} + \nabla \cdot \left(\rho \overrightarrow{V}\right) = 0, \tag{2}$$

$$\frac{\partial \left(\rho \overrightarrow{V}\right)}{\partial t} + \nabla \cdot \left(\rho \overrightarrow{V} \overrightarrow{V}\right) = -\nabla p + \nabla \cdot \left\{\mu \left(\nabla \overrightarrow{V} + \overrightarrow{V}^T\right)\right\} + \rho \overrightarrow{g} + \overrightarrow{F}, \tag{3}$$

$$\frac{\partial \beta}{\partial t} + \overrightarrow{V} \cdot \nabla \beta = 0, \tag{4}$$

where $\overrightarrow{V}$, ρ, μ, p, and $\overrightarrow{F}$ denote the mixture velocity field, the mixture density, the mixture viscosity, the pressure, and the source term that represents the surface tension force, respectively. They can be calculated by Eqs. (5)–(7):

$$\rho = (1-\beta)\,\rho_L + \beta \rho_G, \tag{5}$$

$$\mu = (1-\beta)\,\mu_L + \beta \mu_G, \tag{6}$$

$$\overrightarrow{F} = \sigma \frac{2\rho k_G \nabla \beta}{\rho_G + \rho_L}. \tag{7}$$

k_G is the curvature computed from the divergence of the unit surface normal, and σ is the surface tension. The value of β is between 0 and 1.

The governing equations were solved using finite-volume-based computational fluid dynamics software (FLUENT). The numerical model for mini-channel fluid flow can treat laminar, fluid volume, and unsteady fluid flow. In addition, the SIMPLEC algorithm was applied to solve the pressure velocity coupling. The discretization methods of the gradient, pressure, volume fraction and the momentum were set as Green-Gas Node based of the gradient, PRESTO, Geo-Reconstruct, respectively. For the rectangular mini-channel with a sudden expansion structure, a structured mesh based on the rectangular grid element was utilized. The boundary layer was made near the wall surface. The solutions were considered to be converged when the normalized residual values of all variables were less than 10^{-6}.

A segregated time-dependent unsteady solver was used. The Courant number ranged from 0.25 to 0.27 and the time step ranged between 1×10^{-5} and 1×10^{-6}.

3.2 Computational Domain and Boundary Conditions

Figure 3 illustrates the computational domain, the corresponding coordinate system, and key notations used. The boundary conditions are set as follows.

The velocity inlet is applied at the channel inlet, and

$$X = 0.01 \text{ m}, \quad Y = 0.0125 \text{ m}, \quad w = j = j_G + j_L, \quad u = v = 0, \quad \beta = \frac{x/\rho_G}{x/\rho_G + (1-x)/\rho_L}.$$

j_G and j_L are the gas and liquid superficial velocity of the two-phase flow, respectively.

The pressure outlet is applied at the channel outlet, and

$$X = 0.08 \text{ m}, \quad Y = 0.0125 \text{ m}, \quad P_{out} = 101{,}325 \text{ Pa}.$$

Before the mixture of nitrogen and water is fed to the mini-channel, the mini-channel is filled with water ($\beta = 0$). Besides, there is no heat transfer between the wall of the mini-channel and external environment (26°C, 101,325 Pa).

3.3 Grid Independence Test

Grid independence tests were performed for all mini-channels to determine the optimum mesh and to ensure the reliability of the numerical simulation. The pressure drop and relative errors are

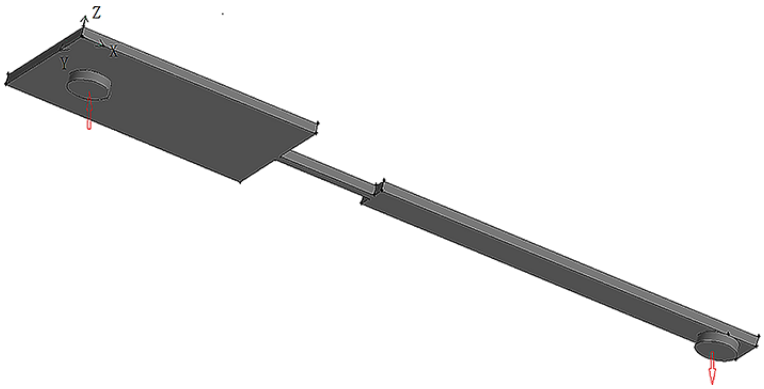

FIG. 3: Computational domain

calculated by Eq. (8) and listed in Table 3. For the sake of higher accuracy and lower computation time, a third type of grid was used in this paper.

$$e = \left| \frac{\Delta P_{\text{sim}} - \Delta P_{\text{exp}}}{\Delta P_{\text{exp}}} \right| \times 100\%. \tag{8}$$

3.4 Data Acquisition

When the two-phase average velocity at the channel was fixed at 1.4 m/s, the gas superficial velocity increased gradually, and the corresponding volume fraction of gas increased from 0.25 to 0.87. The inlet and outlet pressure, phase contour map, and isobar distribution were obtained in the present work. The transient model was used to simulate the transient conditions of the experiments. When the difference between the measured pressure drop and the simulated pressure drop was less than 10% and the simulated flow patterns were similar to the experimental photographs taken by a high-speed camera, the simulations and experiments were considered to be in good agreement.

4. RESULTS AND DISCUSSION

4.1 Pressure Drop Prediction of the Rectangular Mini-Channel with Sudden Expansion

The pressure in the mini-channel module's inlet and outlet plenums were measured by pressure transducers. The compositions of the total pressure drop between the inlet and outlet are shown in Fig. 4.

$$\Delta P_{\text{pred}} = \Delta P_{e1} + \Delta P_{F1} + \Delta P_{c1} + \Delta P_{F2} + \Delta P_{e2} + \Delta P_{F3} + \Delta P_{e3}. \tag{9}$$

TABLE 3: Grid independence test at $w = 0.106$ m/s, $\beta = 0.25$, and $t = 0.1$ s

Grid Number $\times 10^5$	ΔP_{sim} (Pa)	ΔP_{exp} (Pa)	e_{in} (%)
5.92	9962	11306	11.89
10.42	11728		3.74
15.21	11719		3.66

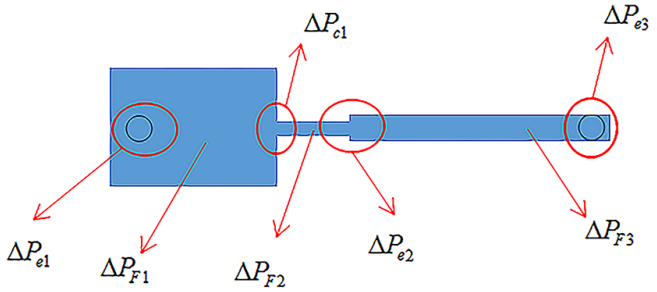

FIG. 4: Components of the total pressure drop

The pressure drop of the sudden contraction as ΔP_{c1} is selected from Chen et al. (2008a), as Eq. (10),

$$\Delta P_{c1} = \Delta P_{cHom} \times (1+\Omega_{c1}) \times (1+\Omega_{c2}) \times (1+\Omega_{c3})^{-0.08}, \tag{10}$$

where

$$\begin{aligned}
\Omega_{c1} &= -0.99e^{(-13.1\times C_1)/C_2}, \\
\Omega_{c2} &= -39.4e^{C_1^{-0.25}}\left(16.1C_3^{-1.5} - 13.2C_3^{-1.8} - 4.2C_3^{-1}\right), \\
\Omega_{c3} &= 0.1C_3^{-13}C_3^{-3}, \\
\Delta P_{cHom} &= \left(\frac{G^2}{2\rho_L}\right)\left[\left(C_c^{-1}-1\right)^2 + \left(1-\sigma_A^2\right)\right]\left[1+x\left(\frac{\rho_L}{\rho_G}-1\right)\right].
\end{aligned} \tag{11}$$

σ_A is the passage cross-section area ratio ($\sigma_A < 1$). The contraction coefficient (C_c) is given as follows:

$$C_c = \frac{1}{0.639\left(1-\sigma_A\right)^{0.5}+1}$$

and

$$C_1 = \mathrm{Bo}^{1.1}(1-x)^{0.9},$$

$$C_2 = 470e - \sigma_A^{-0.2},$$

$$C_3 = \mathrm{We} \times \mathrm{Bo} \times \sigma_A \times (1-x)^{-3},$$

$$C_4 = \sigma_A^{2.5}(1-x)^{-1},$$

where We and Bo are calculated as Eqs. (12) and (13):

$$\mathrm{We} = \frac{G^2 d}{\sigma\rho}, \tag{12}$$

$$\mathrm{Bo} = \frac{\Delta\rho g d^2}{\sigma}. \tag{13}$$

The pressure drop of the sudden expansion as ΔP_{e1}, ΔP_{e2}, ΔP_{e3} are all calculated by Eq. (14):

$$\Delta P_e = \Delta P_{eHom} \times (1+\Omega_{e1}-\Omega_{e2}) \times (1+\Omega_{e3}), \tag{14}$$

where

$$\Delta P_{eHom} = G^2\sigma_A(1-\sigma_A)\left[\frac{(1-x)}{\rho_L} + \frac{x}{\rho_G}\right], \tag{15}$$

$$\Omega_{e1} = \left(\frac{\mathrm{We\,Bo}}{\mathrm{Re}_L}\right) \times \left(\frac{1-x}{x}\right)^{0.3} \times \frac{1}{\mathrm{Fr}^{0.8}}, \tag{16}$$

$$\Omega_{e2} = 0.2 \times \left(\frac{\mu_G}{\mu_L}\right)^{0.4}, \tag{17}$$

$$\Omega_{e3} = 0.4 \times \left(\frac{1-x}{x}\right)^{0.3} + 0.3 \times e^{1.6/\mathrm{Re}_L^{0.1}} - 0.4 \times \left(\frac{\rho_L}{\rho_G}\right)^{0.2}. \tag{18}$$

According to general pressure analysis, the pressure drop of ΔP_{F1}, ΔP_{F2}, ΔP_{F3} can all be written as follows:

$$\Delta P_F = \Delta P_f + \Delta P_a + \Delta P_g, \tag{19}$$

where ΔP_f, ΔP_a, and ΔP_g represent the frictional pressure drop, acceleration pressure drop, and gravitational pressure drop, respectively. For gas-liquid flow in the horizontal channel at room temperature and no phase change in this experiment, there are no gravitational pressure drop and acceleration pressure drop. Therefore,

$$\Delta P_F = \Delta P_f, \tag{20}$$

$$\left(\frac{\Delta p}{\Delta L}\right)_{TP} = \phi_L^2 \left(\frac{\Delta p}{\Delta L}\right)_L, \tag{21}$$

$$\left(\frac{\Delta p}{\Delta L}\right)_L = \frac{2 f_f v_f G^2 (1-x)^2}{D_h}. \tag{22}$$

f_f is calculated by Eq. (23):

$$f_f = 16 \mathrm{Re}_L^{-1}. \tag{23}$$

From Eqs. (20)–(23), it can be seen that the problem of solving the friction pressure drop is transformed into the problem of solving the two-phase friction multiplier ϕ_L^2. Also, the classical Lockhart-Martinelli type correlation could be used as Eq. (24):

$$\phi_L^2 = 1 + \frac{C}{X} + \frac{1}{X^2}. \tag{24}$$

In two-phase flow, the values of X and C are related to the flow regimes of gas and liquid and determined by calculating the Reynolds number utilizing the superficial speed and channel diameter. For both gas and liquid in laminar flow,

$$X_{\mathrm{VV}} = \sqrt{\left(\frac{\Delta p}{\Delta L}\right)_L \Big/ \left(\frac{\Delta p}{\Delta L}\right)_G} = \left(\frac{1-x}{x}\right)^{0.5} \left(\frac{\rho_G}{\rho_L}\right)^{0.5} \left(\frac{\mu_L}{\mu_G}\right)^{0.5}.$$

Carvalho et al. (2020) developed a novel algorithm for flow pattern classification using the vibration signal from a vertical pipe to determine the flow pattern. It indicates that the pressure drop in gas-liquid flow is related to the flow pattern. Fu et al. (2010) have found that the bubble sizes in various regimes could be correlated with several dimensionless numbers such as the ratio of gas/liquid flow rates and capillary number. Wambsganss et al. (1992) also have reported the effect of the flow rate on the two-phase frictional multiplier. From what has been discussed above, it is reasonable to take account of the effects of channel diameter, viscosity, mass velocity, and Reynolds and capillary number in correlation for parameter C. Consequently, C may be expressed as

$$C = f\left(Ca, \mathrm{Re}_L\right).$$

Based on the parameter C prediction model for laminar-laminar flow proposed by Lee and Lee (2001), a new approach, Eq. (25), to predict the parameter C in adiabatic mini-channels is proposed.

$$C = 8.0059 \times 10^{-7} \left(\frac{\mu_L}{D_h G}\right)^{-1.317} Ca^{-0.598} \mathrm{Re}_L^{0.557}, \tag{25}$$

where

$$Ca = \frac{\mu_L G}{\rho_L \sigma}. \tag{26}$$

The value of C is the crucial parameter to calculate the frictional pressure drop. In Figs. 5–9, formulas proposed in other papers are also used to predict the experimental data, and the mean absolute error (MAE) calculated by Eq. (27). Overall results are listed in Table 4.

$$\text{MAE} = \frac{1}{M} \sum \frac{|\Delta P_{\text{pred}} - \Delta P_{\text{exp}}|}{\Delta P_{\text{exp}}} \times 100\%. \tag{27}$$

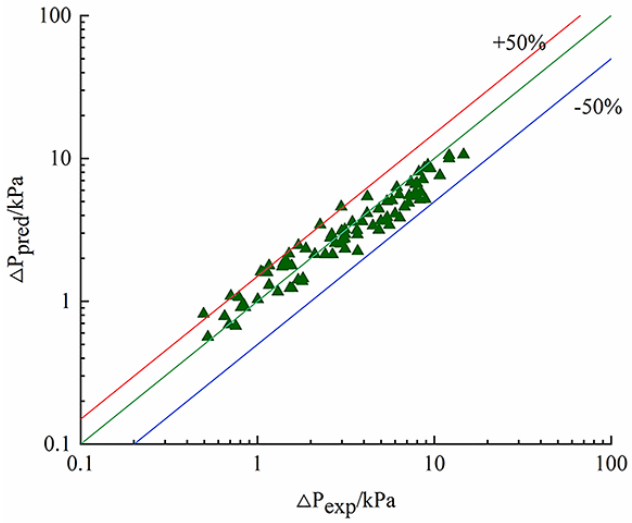

FIG. 5: Comparison of Lockhart and Martinelli (1949) predictions

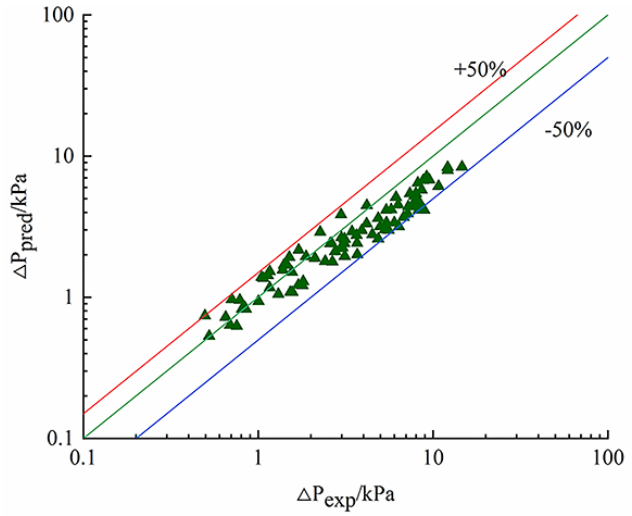

FIG. 6: Comparison of Wambsganss et al. (1992) predictions

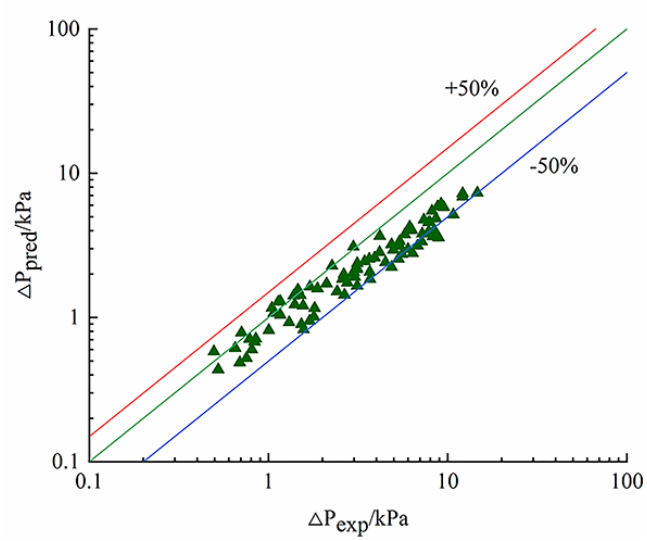

FIG. 7: Comparison of Mishima et al. (1993) predictions

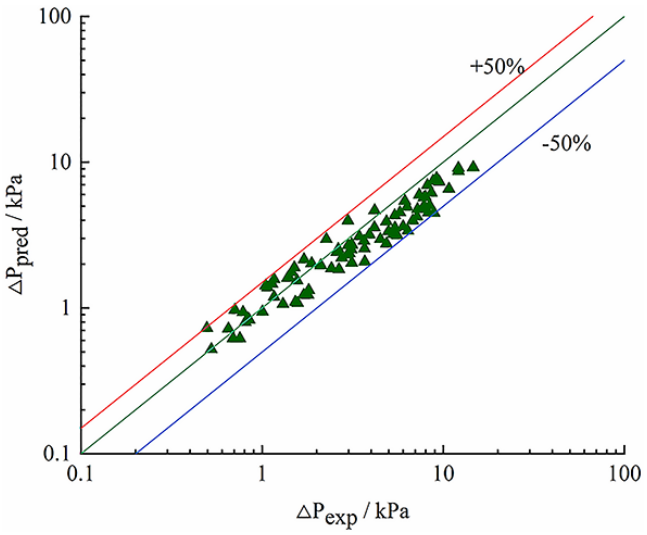

FIG. 8: Comparison of Sun and Mishima (2008) predictions

As shown in Fig. 10, the newly proposed correlation with a mean deviation of 21.3% has better predictive ability than existing correlations.

From Table 4, it seems that the accuracy of the new model is comparable to the formula proposed by Wambsganss et al. (1992). Therefore, in this paper, the two prediction models of parameter C are compared and analyzed using the experimental available data obtained from Lee and Lee (2001) and Liu and Li (2016). Lee and Lee's (2001) experimental data, P^*_{exp}, were obtained under the condition that the working medium was water-air and there was no heat exchange in the flow. Liu and Li's (2016) experimental data, P^*_{exp}, were obtained under the

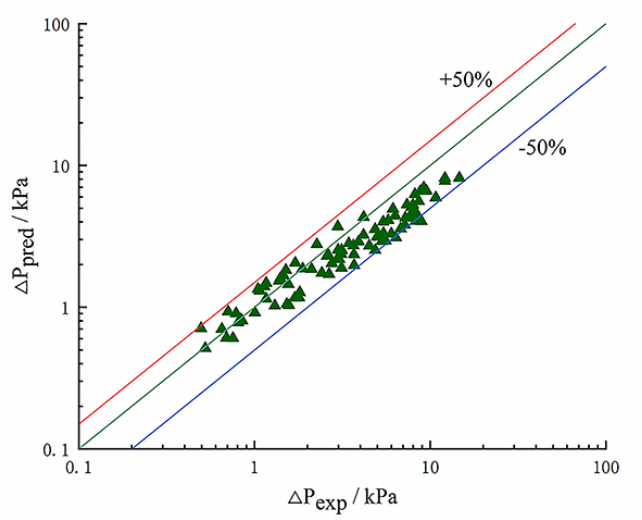

FIG. 9: Comparison of Zhang et al. (2009) predictions

condition that the working medium was R32, R22, or R152a during condensation in a horizontal mini-channel. The results of comparative analysis are shown in Figs. 11 and 12.

From Fig. 11, it can be seen that the range of applications and accuracy of the new prediction formula are better than Wambsganss et al.'s (1992), and from Fig. 12, it can be seen that the accuracy of the new correlation is better than Wambsganss et al.'s (1992) under the condition that the working medium is R32, R22, or R152a during condensation in a horizontal mini-channel. To sum up, the new formula not only has high prediction accuracy, but has a wide range of applications.

4.2 Comparisons of Pressure Drop among Theoretical, Experimental, and Numerical Values

The new theoretical model relating to pressure drop is also validated by experimental data and numerical data. Figure 13 shows the comparisons of pressure drop among theoretical, experimental, and numerical values. As shown in this figure, theoretical data are in good agreement with those obtained from simulation and experiment, with deviation within 10%.

4.3 Study of the Flow Patterns

Figures 14(a)–19(a) show the representative flow images while the corresponding simulations are illustrated in Figs. 14(b)–19(b). β is the volume fraction of gas in the two-phase flow. Five primary flow patterns were identified: bubble flow, slug flow, plug slow, jetlike flow, and annular flow. Compared with the experiments, the absolute error of the pressure drop through the channel obtained from the numerical simulations was within 10%, and the simulated flow patterns were similar to the experimental photographs taken by the high-speed camera. Figure 14 shows that the bubbles in bubbly flow tended to grow just downstream of the sudden expansion position. At the sudden expansion, the cross-sectional area abruptly increases leading to a decline in the velocity and aggregation of bubbles. When the bubbles entered the wider channel, the small

TABLE 4: The MAE when parameter C is used in the existing literature and the present study

Author(s)	Channel Geometry	D_h or gap* width (mm)	Fluid(s)	Test Mode	*C*	MAE (%)
Lockhart and Martinelli (1949)	—	—	—	—	$C_{\mathrm{VV}} = 5$	26.73
Wambsganss et al. (1992)	R, S, H	5.44	air-water	A	$C = 0.15\mathrm{Re}_L^{0.61}$	21.67
Mishima et al. (1993)	R/C, S, V	1.05, 2.05, 3.12, 4.08	air-water	A	$C = 21\left(1 - e^{-0.319 d_e}\right)$	32.04
Sun and Mishima (2008)	R/C/Se, S&M	0.506–12	air-water, R134a, etc.	A	$C_{\mathrm{VV}} = 26\left(1 + \mathrm{Re}_F/1000\right) \times \left[1 - e^{\left(\frac{-0.153}{0.27 N_{\mathrm{conf}} + 0.8}\right)}\right]$	24.22
			water, CO_2, R123, etc.	B		
			R134a	C		
Zhang et al. (2009)	R/C, S&M, H/VU	0.07–6.25	air (N_2)-water, air-ethanol (oil), etc.	A	$C = 21\left(1 - e^{-0.674/Lo*}\right)$ $Lo^* \equiv \{\sigma/[g\left(\rho_f - \rho_g\right)]\}^{0.5}/D_h$	27.37
				B		
New correlation	R, S, H	4×1	Nitrogen-water	A	$C_{\mathrm{VV}} = 8.006 \times 10^{-7} \times \left(\mu_L/(D_h G)\right)^{-1.317} \times Ca^{-0.598}\mathrm{Re}_{Fo}^{0.557}$	21.3

C: circular; R: rectangular; H: horizontal; VU: vertical upward; A: adiabatic; B: boiling; C: condensing; S: single; M: multi; Se: semi-triangular

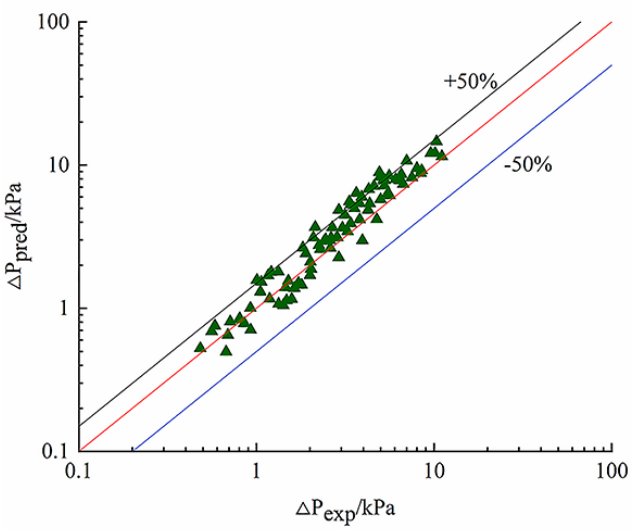

FIG. 10: Comparison between the experimental measurements and the new Chisholm parameter (C) correlation

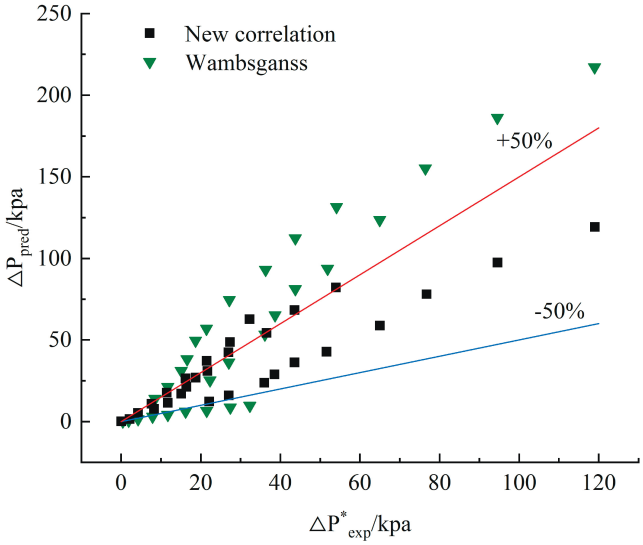

FIG. 11: Comparison between Wambsganss et al.'s correlation (1992) and the new correlation using experimental data from the open literature (Lee and Lee, 2001)

bubbles coalesced into larger ones. With the increase in gas content, the bubbles continued to grow until the large bubbles became a large oblong bubble (slug) which is separated by a liquid slug, and then the slug flow appeared as in Fig. 15. As the gas content continued to increase, the shear force of the liquid on the bubbles became greater than their surface tension, which caused the bubbles to burst at the tail of the plug, resulting in plug flow, as shown in Fig. 16. As the quantity of gas further increased, the entering flow gained enough momentum to become

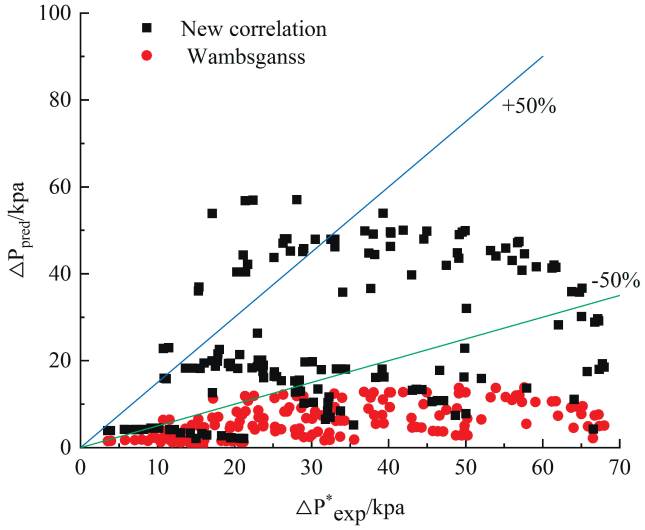

FIG. 12: Comparison between Wambsganss et al.'s correlation (1992) and the new correlation using experimental data from the open literature (Liu and Li, 2016)

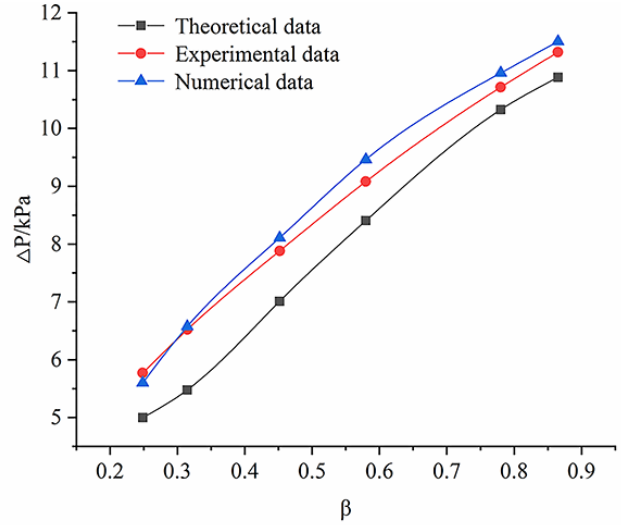

FIG. 13: Comparisons of pressure drop among theoretical, experimental, and numerical values

a jetlike flow that could break through the front bubble, gas slug, or other complex gas forms (Fig. 17). In the meantime, an increase in pressure at the position of the sudden expansion was similar to what Chen et al. (2007) found, as shown in Fig. 18. Again, it shows the validity of the simulations. As the gas continued to increase, the kinetic energy of the incoming fluid fully broke through the channel and eventually formed an annular flow (Fig. 19). From Figs. 14(c)–19(c), which are isobar distribution of flow patterns, it can be seen that the pressure gradients on the bubble surface are very large. Thus, the pressure drop of gas-liquid flow is closely related to the flow pattern.

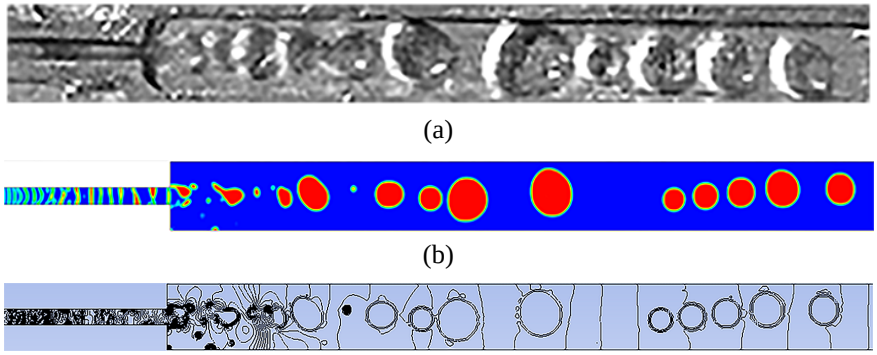

(a)

(b)

(c)

FIG. 14: Bubble flow at $j_G = 0.356$ m/s, $j_L = 1.050$ m/s, $t = 0.1$ s. (a) Image of the bubble flow, (b) simulation of the bubble flow, (c) isobar of bubble flow.

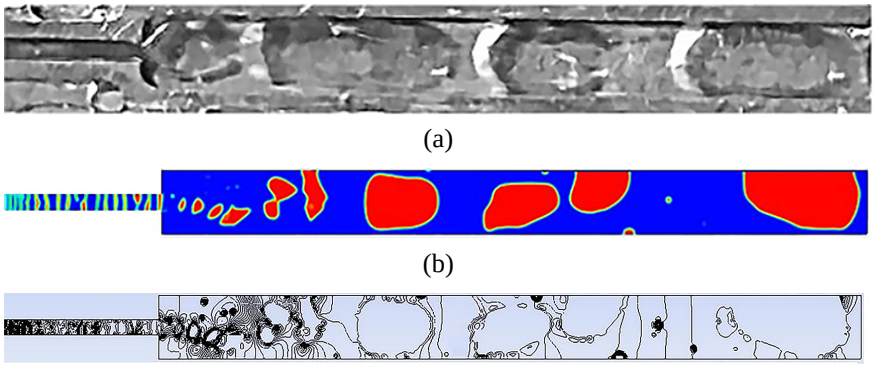

(a)

(b)

(c)

FIG. 15: Slug flow at $j_G = 0.448$ m/s, $j_L = 0.952$ m/s, $t = 0.1$ s. (a) Image of the slug flow, (b) simulation of the the slug flow, (c) isobar of slug flow.

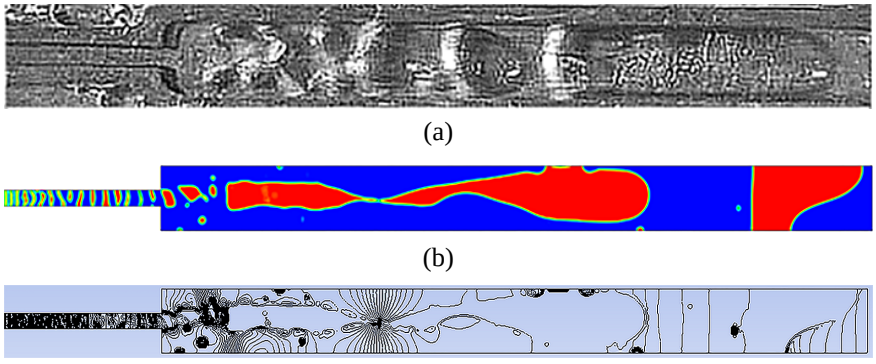

(a)

(b)

(c)

FIG. 16: Plug flow at $j_G = 0.63$ m/s, $j_L = 0.77$ m/s, $t = 0.1$ s. (a) Image of the plug flow, (b) simulation of the the plug flow, (c) isobar of plug flow.

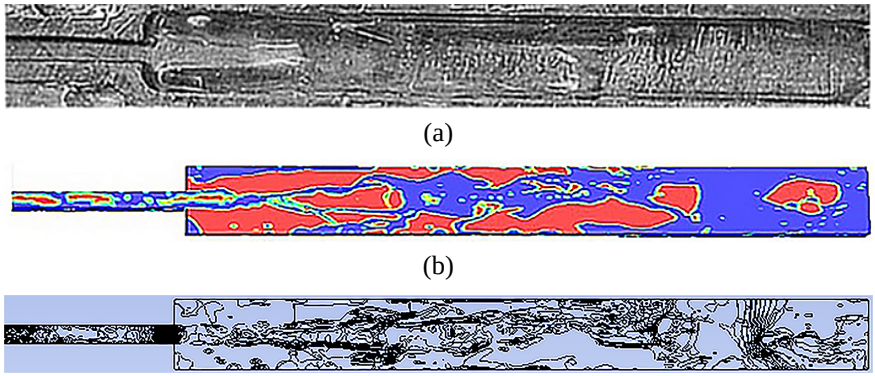

(a)

(b)

(c)

FIG. 17: Jetlike flow at $j_G = 0.812$ m/s, $j_L = 0.588$ m/s, $t = 0.1$ s. (a) Image of the jetlike flow, (b) simulation of the jetlike flow, (c) isobar of jetlike flow.

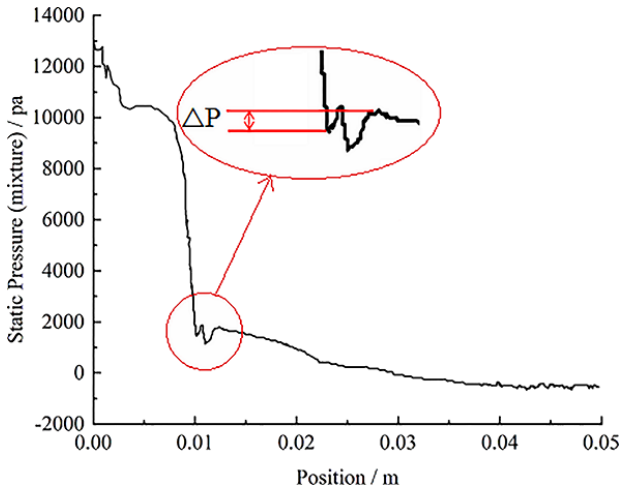

FIG. 18: Jetlike flow pressure drop distribution at central axis

5. CONCLUSIONS

This study investigated two-phase flow characteristics in a rectangular mini-channel with sudden expansion structure by experiments and numerical simulations. The frictional pressure drop prediction formula accurately predicted 120 experimental data points, while the flow patterns in the mini-channel were captured by the high-speed camera. The conclusions obtained are as follows:

1. Five primary flow patterns were identified from the experiments and simulations: bubble flow, slug flow, plug flow, jetlike flow and annular, flow. The pressure distribution along the central axis suggests that an appreciable increase in pressure occurs at the position of the expansion when the jetlike flow is pronounced.

2. The pressure gradient on the bubble surface is very large and the pressure drop of the gas-liquid flow is closely related to the flow pattern.

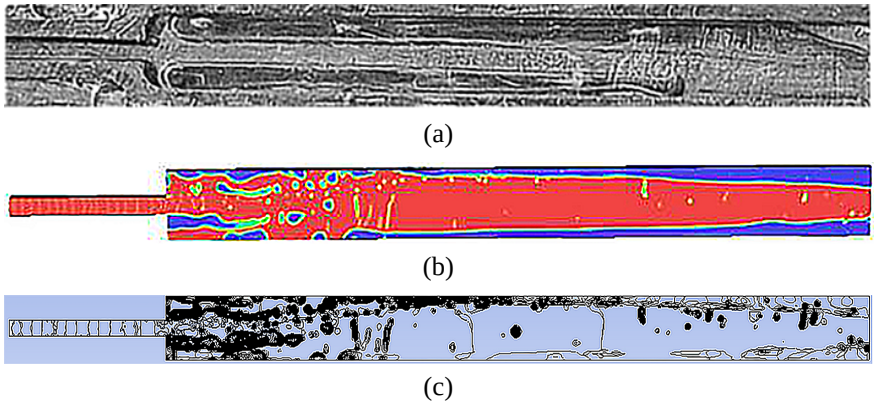

FIG. 19: Annular flow at $j_G = 1.218$ m/s, $j_L = 0.182$ m/s, $t = 0.1$ s. (a) Image of the annular flow, (b) simulation of the annular flow, (c) isobar of annular flow.

3. The dimensionless parameter Ca is introduced, and a new correlation accounting for the effects of small channel diameter, viscosity, surface tension, mass velocity, flow patterns, and flow regimes for parameter C is proposed. The new correlation was used to predict the two-phase frictional pressure drop in a single rectangular mini-channel with sudden expansion structure. The results show that the MAE reached 21.3%.

ACKNOWLEDGMENT

This work is supported by the Natural Science Foundation of Hebei Province, China, under Grant No. E2019210036.

REFERENCES

Abdelall, F.F., Hahm, G., Ghiaasiaan, S.M., Abdel-Khalik, S.I., Jeter, S.S., Yoda, M., and Sadowski, D.L., Pressure Drop Caused by Abrupt Flow Area Changes in Small Channels, *Exp. Therm. Fluid Sci.*, vol. **29**, no. 4, pp. 425–434, 2004.

Abood, S.A., Abdulwahid, M.A., and Almudhaffar, M.A., Comparison between the Experimental and Numerical Study of (Air-Oil) Flow Patterns in Vertical Pipe, *Case Studies Therm. Eng.*, vol. **14**, p. 100424, 2019.

Ahmed, W.H., Ching, C.Y., and Shoukri, M., Pressure Recovery of Two-Phase Flow across Sudden Expansions, *Int. J. Multiphase Flow*, vol. **33**, no. 6, pp. 575–594, 2006.

Alejandro, L.B., Francisco, V.G., and Jose, R.G.C., Non-Uniform Condensation of Refrigerant R134A in Mini-Channel Multiport Tubes: Two-Phase Pressure Drop and Heat Transfer Coefficient, *J. Enhanced Heat Transf.*, vol. **22**, no. 5, pp. 391–416, 2015.

Attou, A. and Bolle, L., A New Correlation for the Two-Phase Pressure Recovery Downstream from a Sudden Enlargement, *Chem. Eng. Technol.*, vol. **20**, no. 6, pp. 419–423, 1997.

Carvalho, F.C.T., Figueiredo, M.M.F., and Serpa, A.L., Flow Pattern Classification in Liquid-Gas Flows Using Flow-Induced Vibration, *Exp. Therm. Fluid Sci.*, vol. **112**, p. 109950, 2020.

Chai, L., Xia, G.D., and Wang, H.S., Laminar Flow and Heat Transfer Characteristics of Interrupted Microchannel Heat Sink with Ribs in the Transverse Microchambers, *Int. J. Therm. Sci.*, vol. **110**, pp. 1–11, 2016.

Chen, Y., Liu, C.C., Chien, K.H., and Wang, C.C., Two-Phase Flow Characteristics across Sudden Expansion in Small Rectangular Channels, *Exp. Therm. Fluid Sci.*, vol. **32**, no. 2, pp. 696–706, 2007.

Chen, Y., Chu, M.C., Liaw, J.S., and Wang, C.C., Two-Phase Flow Characteristics across Sudden Contraction in Small Rectangular Channels, *Exp. Therm. Fluid Sci.*, vol. **32**, no. 8, pp. 1609–1619, 2008a.

Chen, Y., Tseng, C.Y., Lin, Y.T., and Wang, C.C., Two-Phase Flow Pressure Change Subject to Sudden Contraction in Small Rectangular Channels, *Int. J. Multiphase Flow*, vol. **35**, no. 3, pp. 297–306, 2008b.

Choi, C.W., Yu, D.I., and Kim, M.H., Adiabatic Two-Phase Flow in Rectangular Microchannels with Different Aspect Ratios: Part I—Flow Pattern, Pressure Drop and Void Fraction, *Int. J. Heat Mass Transf.*, vol. **54**, no. 1, pp. 616–624, 2010.

English, N.J. and Kandlikar, S.G., An Experimental Investigation into the Effect of Surfactants on Air-Water Two-Phase Flow in Minichannels, *Heat Transf. Eng.*, vol. **27**, no. 4, pp. 99–109, 2006.

Fu, T.T., Ma, Y.G., Funfschilling, D., Zhu, C., and Li, H.Z., Squeezing-to-Dripping Transition for Bubble Formation in a Microfluidic T-Junction, *Chem. Eng. Sci*., vol. **65**, no. 12, pp. 3739–3748, 2010.

Guan, N., Jiang, G.L., Liu, Z.G., and Zhang, C.W., Flow and Heat Transfer in Hydrophobic Micro Pin Fins with Different Contact Angles, *Heat Transf. Res.*, vol. **50**, no. 8, pp. 799–820, 2019.

Guo, Z.X., Heat Transfer Enhancement—A Brief Review of 2018 Literature, *J. Enhanced Heat Transf.*, vol. **26**, no. 5, pp. 429–449, 2019.

Heyhat, M.M., Kowsary, F., Rashidi, A.M., Momenpour, M.H., and Amrollahi, A., Experimental Investigation of Laminar Convective Heat Transfer and Pressure Drop of Water-Based Al_2O_3 Nanofluids in Fully Developed Flow Regime, *Exp. Therm. Fluid Sci.*, vol. **44**, pp. 483–489, 2013.

Kim, S.M. and Mudawar, I., Universal Approach to Predicting Two-Phase Frictional Pressure Drop for Adiabatic and Condensing Mini/Micro-Channel Flows, *Int. J. Heat Mass Transf.*, vol. **55**, nos. 11-12, pp. 3246–3261, 2012.

Kumar, V. and Sarkar, J., Numerical and Experimental Investigations on Heat Transfer and Pressure Drop Characteristics of Al_2O_3–TiO_2 Hybrid Nanofluid in Minichannel Heat Sink with Different Mixture Ratio, *Powder Technol*., vol. **345**, pp. 717–727, 2019.

Kumar, V. and Sarkar, J., Two-Phase Numerical Simulation of Hybrid Nanofluid Heat Transfer in Minichannel Heat Sink and Experimental Validation, *Int. Commun. Heat Mass Transf.*, vol. **91**, pp. 239–247, 2018.

Lee, H.J. and Lee, S.Y., Pressure Drop Correlations for Two-Phase Flow within Horizontal Rectangular Channels with Small Heights, *Int. J. Multiphase Flow*, vol. **27**, no. 5, pp. 783–796, 2001.

Lee, S., Devahdhanush, V.S., and Mudawar, I., Pressure Drop Characteristics of Large Length-to-Diameter Two-Phase Micro-Channel Heat Sinks, *Int. J. Heat Mass Transf.*, vol. **115**, pp. 1258–1275, 2017.

Lei, Y.C. and Chen, Z.Q., Numerical Study of Condensation Flow Regimes in Presence of Non-Condensable Gas in Minichannels, *Int. Commun. Heat Mass*, vol. **106**, pp. 1–8, 2019.

Liu, N. and Li, J.M., Experimental Study on Pressure Drop of R32, R152a, and R22 during Condensation in Horizontal Minichannels, *Exp. Therm. Fluid Sci*., vol. **71**, pp. 14–24, 2016.

Li, X.J. and Hibiki, T., Frictional Pressure Drop Correlation for Two-Phase Flows in Mini and Micro Single-Channels, *Int. J. Multiphase Flow*, vol. **90**, pp. 29–45, 2017.

Lockhart, R.W. and Martinelli, R.C., Proposed Correlation of Data for Isothermal Two-Phase, Two-Component Flow in Pipes, *Chem. Eng. Prog.*, vol. **45**, pp. 39–48, 1949.

Mishima, K., Hibiki, T., and Nishihara, H., Some Characteristics of Gas-Liquid Flow in Narrow Rectangular Duct, *Int. J. Multiphase Flow*, vol. **19**, no. 1, pp. 115–124, 1993.

Moffat, R.J., Describing the Uncertainties in Experimental Results, *Exp. Therm. Fluid Sci.*, vol. **1**, no. 1, pp. 3–17, 1988.

Nandakrishnan, S.L., Deepu, M., and Shine, S.R., Numerical Investigation of Heat-Transfer Enhancement in a Dimpled Diverging Microchannel with Al_2O_3-Water Nanofluid, *J. Enhanced Heat Transf.*, vol. **25**,

nos. 4-5, pp. 347–365, 2018.

Qu, W. and Siu-Ho, A., Measurement and Prediction of Pressure Drop in a Two-Phase Micro-Pin-Fin Heat Sink, *Int. J. Heat Mass Transf.*, vol. **52**, no. 21, pp. 5173–5184, 2009.

Sahar, A.M., Wissink, J., Mahmoud, M.M., Karayiannis, T.G., and Ishak, M.S.A., Effect of Hydraulic Diameter and Aspect Ratio on Single Phase Flow and Heat Transfer in a Rectangular Microchannel, *Appl. Therm. Eng*., vol. **115**, pp. 793–814, 2017.

Schmidt, J. and Friedel, L., Two-Phase Flow Pressure Drop across Sudden Contractions in Duct Areas, *Int. J. Multiphase Flow*, vol. **23**, no. 2, pp. 283–299, 1997.

Schmidt, J. and Friedel, L., Two-Phase Flow Pressure Change across Sudden Expansions in Duct Areas, *Chem. Eng. Commun*., vol. **141**, no. 1, pp. 175–190, 1994.

Sempértegui-Tapia, D.F. and Ribatski, G., Two-Phase Frictional Pressure Drop in Horizontal Micro-Scale Channels: Experimental Data Analysis and Prediction Method Development, *Int. J. Refrig*., vol. **79**, pp. 143–163, 2017.

Sun, L.C. and Mishima, K., Evaluation Analysis of Prediction Methods for Two-Phase Flow Pressure Drop in Mini-Channels, *Int. J. Multiphase Flow*, vol. **35**, no. 1, pp. 47–54, 2008.

Tiwari, N. and Manoj, K.M., Numerical Study of Thermal Enhancement in Modified Raccoon Microchannels, *Heat Transf. Res.*, vol. **50**, no. 6, pp. 519–543, 2019.

Wadle, M.A., New Formula for the Pressure Recovery in an Abrupt Diffuser, *Int. J. Multiphase Flow*, vol. **15**, no. 2, pp. 241–256, 1989.

Wambsganss, M.W., Jendrzejczyk, J.A., France, D.M., and Obot, N.T., Frictional Pressure Gradients in Two-Phase Flow in a Small Horizontal Rectangular Channel, *Exp. Therm. Fluid Sci.*, vol. **5**, no. 1, pp. 40–56, 1992.

Wang, C.C., Tseng, C.Y., and Chen, I.Y., A New Correlation and the Review of Two-Phase Flow Pressure Change across Sudden Expansion in Small Channels, *Int. J. Heat Mass Transf.*, vol. **53**, no. 19, pp. 4287–4295, 2010.

Wei, L., Pan, L.M., Zhao, Y.M., Ren, Q.Y., and Zhang, W.Z., Numerical Study of Adiabatic Two-Phase Flow Patterns in Vertical Rectangular Narrow Channels, *Appl. Therm. Eng*., vol. **110**, pp. 1101–1110, 2017.

Wu, W., Xiao, B.Q., Hu, J., Yuan, S., and Hu, C.H., Experimental Investigation on the Air-Liquid Two-Phase Flow inside a Grooved Rotating-Disk System: Flow Pattern Maps, *Appl. Therm. Eng*., vol. **133**, pp. 33–38, 2018.

Xiao, Y., Hu, Z.X., Chen, S., and Gu, H., Experimental Study of Two-Phase Frictional Pressure Drop of Steam-Water in Helically Coiled Tubes with Small Coil Diameters at High Pressure, *Appl. Therm. Eng*., vol. **132**, pp. 18–29, 2018.

Zhai, Y.L., Xia, G.D., Li, Z.H., and Wang, H., Experimental Investigation and Empirical Correlations of Single and Laminar Convective Heat Transfer in Microchannel Heat Sinks, *Exp. Therm. Fluid Sci.*, vol. **83**, pp. 207–214, 2017.

Zhang, W., Hibiki, T., and Mishima, K., Correlations of Two-Phase Frictional Pressure Drop and Void Fraction in Mini-Channel, *Int. J. Heat Mass Transf.*, vol. **53**, no. 1, pp. 453–465, 2009.